VERSION NOVEMBER 12, 2025
Preprint typeset using LaTeX style openjournal v. 09/06/15

EFFECT OF IONIZING PHOTON ESCAPE FRACTION IN FAINT GALAXIES ON MODELING REIONIZATION HISTORY OF THE UNIVERSE

ZEWEI WU [1,2★], ANDREY KRAVTSOV [1,3,4,†], AND HARLEY KATZ [1,3]

[1]Department of Astronomy & Astrophysics, The University of Chicago, Chicago, IL 60637 USA
[2]Department of Astronomy & Astrophysics, University of California, San Diego, La Jolla, CA 92093 USA
[3]Kavli Institute for Cosmological Physics, The University of Chicago, Chicago, IL 60637 USA and
[4]Enrico Fermi Institute, The University of Chicago, Chicago, IL 60637 USA
Version November 12, 2025

ABSTRACT

We present model calculations of the reionization history of hydrogen using star formation histories, computed with a galaxy formation model which reproduces properties of local dwarf galaxies and UV luminosity functions of galaxies at $z = 5 - 16$. We use the ionizing photon density functions predicted by the model along with different models for the escape fraction of ionizing photons, $f_{\rm esc}$, to study the effects of ionizing photons from faint galaxies and different assumptions about $f_{\rm esc}$ on the evolution of hydrogen ionized fraction with redshift, $Q_{\rm HII}(z)$. We show that accounting for the contribution of faint galaxies with UV luminosities $M_{1500} > -13$, and with a *constant* ionizing photon escape fraction of $f_{\rm esc} = 0.1$ results in the hydrogen reionization history consistent with all current observational constraints. Comparing results of the $f_{\rm esc} = 0.1$ model and two alternative models shows that the model with a strong luminosity dependence of $f_{\rm esc}$, which assigns high $f_{\rm esc}$ to faint galaxies, results in early reionization inconsistent with observational constraints. However, the model in which $f_{\rm esc}$ follows a universal redshift-independent correlation with the recent maximum specific star formation rate, motivated by the results of the SPHINX galaxy formation simulation, results in the reionization history in good agreement with existing observational constraints, even though this model produces a sizeable ionized hydrogen fraction of $Q_{\rm HII} \approx 0.15 - 0.2$ at redshifts $z = 8 - 12$. Our results show that the relative contribution of faint dwarf galaxies to reionization depends sensitively on assumptions about the escape fraction for galaxies of different luminosities, and that this is the main source of uncertainty in modeling hydrogen reionization.

Subject headings: galaxies: luminosity function; galaxies: reionization; galaxies: formation; galaxies: dwarf; galaxies: halos

1. INTRODUCTION

Ever since Gunn & Peterson (1965) pointed out that transmission of the rest-frame UV emission in quasar spectra indicates that the intergalactic hydrogen is in a highly ionized state, an ever-increasing body of observations has revealed that the intergalactic gas transitioned from neutral to ionized state around redshift $z \approx 6$ (e.g., Becker et al. 2001; Gnedin 2004; Gnedin & Fan 2006, see Robertson 2022; Gnedin & Madau 2022 for reviews). Both observations and cosmological simulations show that this process of *reionization* was dominated by the ionizing photons from young star-forming galaxies (e.g., Gnedin 2000; Gnedin & Kaurov 2014; Ma et al. 2015; Robertson et al. 2015; Sharma et al. 2016; Madau 2017; Lewis et al. 2023), with active galactic nuclei (AGNs) playing a key role in helium reionization at $z < 4$ and maintaining the intergalactic medium (IGM) ionized at lower redshifts (e.g., Sokasian et al. 2003).

It is still not entirely clear which galaxies dominate the reionization of hydrogen at $z \approx 6$. This is partly because the ionizing photon flux cannot be directly observed, and needs to be estimated with a number of assumptions from the observed UV emission. Besides, the contribution of galaxies with UV absolute magnitudes at $\lambda = 1500$ Å, or $M_{1500} > -14$ to the UV flux budget is unconstrained by observations. For example, opposite conclusions have been reached about the relative importance of bright and faint galaxies to the reionization of the Universe, due to different assumptions about ionizing photon contribution from galaxies of different luminosities (e.g., Finkelstein et al. 2019; Naidu et al. 2020). Assumptions of high escape fraction in dwarf galaxies, on the other hand, have been shown to result in early reionization scenarios inconsistent with observational constraints (Muñoz et al. 2024).

Theoretical models and simulations, likewise, are plagued by uncertainties related to the challenge of correctly modeling the entire spectrum of galaxy masses (e.g., Gnedin et al. 2008; O'Shea et al. 2015; Gnedin 2016; Yue et al. 2016; Kannan et al. 2022), and face the even more challenging problem of modeling escape of ionizing radiation from galaxies (e.g., Rosdahl et al. 2022).

In a recent study, we used a model that reproduces the observed properties of both low-redshift dwarf galaxies and the UV luminosity function of galaxies at $z \approx 5 - 13$ to investigate the potential contribution of faint galaxies to the UV and ionizing photon budgets (Wu & Kravtsov 2024). We showed that the contribution of galaxies with $M_{1500} > -14$ to the UV flux and ionizing photon budget is $\approx 40 - 60\%$ at $z > 7$ and decreases to $\approx 20\%$ at $z = 6$ if one assumes that escape fraction of ionizing photons is independent of galaxy luminosities. The contribution of dwarf galaxies is potentially larger if their ionizing photon escape fractions are larger than those of brighter galaxies. These results indicated that dwarf galaxies fainter than the observational limit at $z > 5$ can contribute significantly to the UV flux density and ionizing photon budget.

★jaw064@ucsd.edu or wu@ucsd.edu, †kravtsov@uchicago.edu

In this follow-up study, we present calculations of the reionization history of the Universe using the same galaxy formation model and several assumptions about the escape fraction of ionizing photons in galaxies of different luminosity. The calculation of ionizing fluxes of galaxies is done as described in Wu & Kravtsov (2024), but we extend our modeling of galaxies to $z \approx 16$, and demonstrate that the model reproduces existing estimates of the UV luminosity function (LF) at $5 < z < 16$ relevant for robust modeling of reionization. The evolution of the ionized fraction of the intergalactic hydrogen is carried out using the model of Madau et al. (1999, with some modifications detailed in Madau 2017). We show that assumptions about escape fraction from galaxies are the *largest* uncertainty factor in theoretical modeling of reionization – far larger than modeling the relative contribution of ionizing photons by galaxies of different luminosities, or uncertainties related to the clumping factor of the intergalactic gas. In particular, we show that within a range of reasonable approaches to modeling escape fraction, a wide range of reionization histories can be obtained, including histories in good agreement with existing observational constraints on the hydrogen ionized fraction and Thomson optical depth.

The paper is organized as follows. We describe the galaxy formation model, and the range of adopted models for the escape fraction of ionizing radiation in Section 2. We present our main results in Section 3, and discuss their implications in Section 4. Our results and conclusions are summarized in Section 5. We provide parameters for our stochastic star formation model in Appendix B and fitting functions to both the UV LF and ionizing photon abundance in Appendices C and D.

Throughout this paper, we assume flat Λ+Cold Dark Matter (ΛCDM) cosmology with the mean density of matter in units of the critical density of $\Omega_{\rm m} = 0.32$, the mean density of baryons of $\Omega_{\rm b} = 0.045$, Hubble constant of $H_0 = 67.11\,{\rm km\,s^{-1}\,Mpc^{-1}}$, the amplitude of fluctuations within the tophat spheres of $R = 8h^{-1}$ Mpc of $\sigma_8 = 0.82$ (where h is the reduced Hubble constant), and the primordial slope of the power spectrum of $n_{\rm s} = 0.95$.

2. MODELING HIGH-Z GALAXY FORMATION

The galaxy formation framework we use in this study is applied to predict galaxy population properties for representative samples of model galaxies at all relevant luminosities down to UV absolute magnitudes of $M_{1500} \approx -5$ and redshifts $z \in [5, 16]$. This is done using samples of halos that follow the expected halo mass function at each considered redshift and halo mass evolution tracks constructed using an accurate approximation for the halo mass accretion rate, as described in Kravtsov & Belokurov (2024).

The key aspect of the galaxy formation model we use in this study at $z \geq 5$ is that it reproduces observed properties of sub-L_* galaxies at $z = 0$ down to the faintest ultra-faint dwarf galaxies (Kravtsov & Manwadkar 2022; Manwadkar & Kravtsov 2022; Kravtsov & Wu 2023; Pan & Kravtsov 2023). This agreement is not a guarantee that the model would work at high redshifts. Nevertheless, most galaxies at $z > 5$ have dwarf halo virial masses ($M_{\rm 200c} \lesssim 10^{11}\,M_\odot$) similar to that of $z = 0$. Therefore, the agreement at $z = 0$, as well as the successful forward modeling of $5 \leq z \leq 10$ UV LF in Wu & Kravtsov (2024), give us more confidence that results may be realistic for higher redshifts. Although the model requires increasing stochasticity of star formation rate with increasing redshift to match the observed UV luminosity function at $z > 5$ (Kravtsov & Belokurov 2024), models with such increased stochasticity are consistent with most observed properties of $z = 0$ dwarf galaxies (Pan & Kravtsov 2023).

2.1. *Halo evolution and star formation model*

To model the evolution of galaxies over the entire relevant range of galaxy luminosities, we first construct large samples of model halos using the approach described in Kravtsov & Belokurov (2024), with specific choices for modeling reionization detailed in Wu & Kravtsov 2024, and adjustments for $z \geq 10$ galaxies in Appendix B. Specifically, halo samples over a broad range of masses, required to cover the entire relevant range of luminosities, are drawn from a series of cubic volumes of increasing size. A mass assembly history for each halo is generated using an accurate approximation for the halo mass accretion history, presented in the Appendix of Kravtsov & Belokurov (2024).

The mass assembly history is then used to construct galaxy evolution track using the model of Kravtsov & Manwadkar (2022) with modifications to account for stochasticity of star formatin rate (Pan & Kravtsov 2023; Kravtsov & Belokurov 2024). Specifically, the SFR in the model at time t_n is perturbed as $\dot{M}_{\star,\rm stoch} = \dot{M}_\star \times 10^{\Delta}$, where Δ is the a correlated random number drawn from a Gaussian distribution with zero mean and unit variance. The number Δ is modulated to include time correlations by scaling it with $\sqrt{P(k)} = \sqrt{{\rm PSD}(f_k)/T}$ (see Pan & Kravtsov 2023, for details), where the power spectral density (PSD) depends on the temporal frequency f_k, T is the duration of the galaxy's evolutionary track, and the corresponding wavenumber is defined as $k = f_k T$. Following Tacchella et al. (2020) we use the PSD of the form ${\rm PSD}(f) = \sigma_\Delta^2[1 + (\tau_{\rm break} f)^\alpha]^{-1}$, where σ_Δ characterizes the amplitude of the SFR variability over long time scales and $\tau_{\rm break}$ characterizes the timescale over which the random numbers are effectively uncorrelated. Parameter α controls the slope of the PSD at high frequencies (short time scales). We note that Pan & Kravtsov (2023) explicitly showed that adding SFR stochasticity improves agreement of the model with observations of local dwarf galaxies.

For each halo track produced as described above, the galaxy formation model is integrated from $z_{\rm init} = 25$ to the final redshift $z_{\rm f} = 5, 6, 7, 8, 9, 10$, and from $z_{\rm init} = 35$ for $z_{\rm f} = 11, 12, 13, 14, 16$ to ensure the halo tracks are integrated for enough time, producing the evolution of stellar mass, star formation rate, etc. We tested each of the initial redshift values for convergence of the resulting luminosity and ionizing flux functions.

2.2. *Computing UV and ionizing radiation luminosities*

The monochromatic luminosity of model galaxies at $\lambda = 1500\,$Å is computed using a tabulated grid of luminosities, L_{1500}, for stellar populations of a given age and metallicity using the Flexible Stellar Population Synthesis model v3.0 (FSPS, Conroy et al. 2009; Conroy & Gunn 2010b) and its Python bindings, Python-FSPS. The table is then used to construct an accurate bivariate spline approximation to compute L_{1500} for stellar populations of a given age and metallicity. We use the table and finely spaced time outputs of the model to compute the integral L_{1500} due to all stars formed by the current time taking into account the evolution of stellar mass and stellar metallicity.

The emission rate of LyC photons with $\lambda < 912\,$Å, $\dot{N}_{\rm ion}$, is

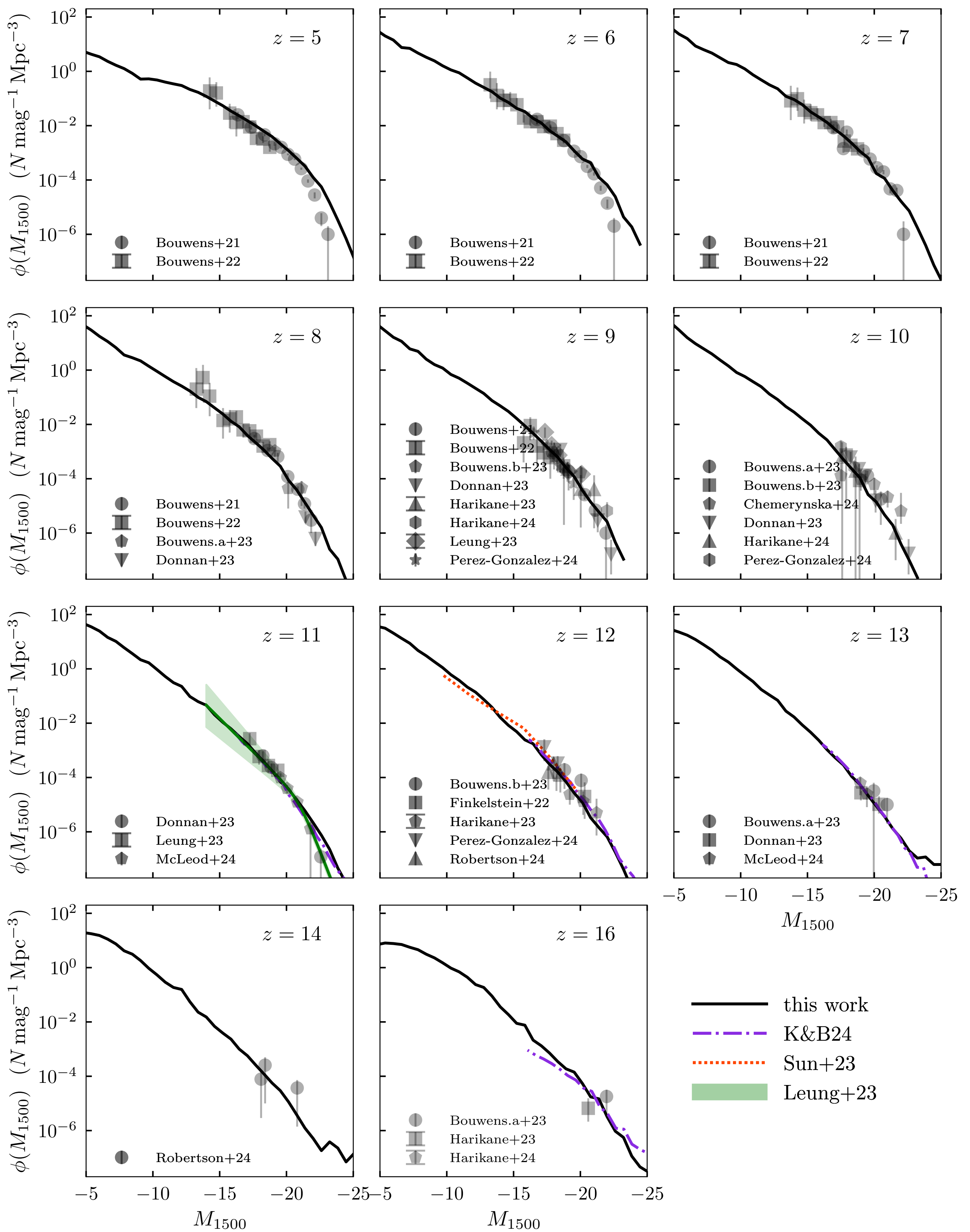

FIG. 1.— Rest-frame UV luminosity function of galaxies in the GRUMPY model with specific modifications for modeling reionization detailed in Wu & Kravtsov 2024; Kravtsov & Belokurov 2024 (see Appendix B), each panel showing a redshift at $z \in [5, 16]$. Effects of dust are not included in the model LFs (see §2.3 of Wu & Kravtsov 2024). The different symbols show observational estimates of the UV LF in recent studies that used HST and JWST observations (Bouwens et al. 2021, 2022; Finkelstein et al. 2022; Bouwens et al. 2023a,b; Donnan et al. 2023; Harikane et al. 2023; Leung et al. 2023; Harikane et al. 2024; McLeod et al. 2024; Pérez-González et al. 2023; Robertson et al. 2024). Theoretical models are shown in dashed (Sun et al. 2023), dash-dotted (Kravtsov & Belokurov 2024) lines and colored regions (Leung et al. 2023). Note that before reionization (i.e. $z \gtrsim 6$), the slope of the LF even at the faintest magnitudes remains as steep as the slope at $M_{1500} \approx -14$. For a single-panel comparison of UV LF evolution over redshift, see Fig. 2 of Wu & Kravtsov (2024).

computed using ionizing flux tables from the BPASS version 2.3 models (Byrne et al. 2022), which take into account the effect of binary stars, and the evolution of stellar mass and metallicity computed by the galaxy formation model. We neglect the effects of dust, which affect only a limited range of bright luminosities at $z \lesssim 7$ (see Fig. 1 in Wu & Kravtsov 2024). The UV luminosity and ionizing photon flux functions of model galaxies are then constructed using a weighted contribution of objects from different cubic volumes. We computed the ionizing flux contributions for all galaxies with the monochromatic UV absolute magnitudes at $\lambda = 1500$ of $M_{1500} < -5$, for the reasons discussed in §2 of our previous paper (Wu & Kravtsov 2024, where we refer the reader for other modeling details):

$$\langle \dot{n}_{\rm ion} \rangle = \int_{-\infty}^{-5} \frac{d\dot{n}_{\rm ion}}{dM_{1500}}\, dM_{1500}, \qquad (1)$$

The UV luminosity functions produced with this method over a range of absolute magnitudes $-25 \lesssim M_{1500} \leq -5$ and redshift range $z = 5 - 16$ are shown as black solid lines in Figure 1 and compared to existing observational estimates. In our model, the end of reionization GRUMPY parameter is set to $z_{\rm rei} = 6$ (see §3.2 of Wu & Kravtsov 2024). As discussed, we adopt a stochastic SFR model in line with Kravtsov & Belokurov (2024), with specific values of σ_Δ for each redshift presented in Appendix B. Best-fit parameters of the modified Schechter function fits to the UV luminosity and ionizing flux functions are also provided in Appendix C.

Figure 1 shows that the model captures the shape and evolution of the UV luminosity function across the luminosity and redshift range probed by observations. Differences at $z \leq 7$ and $M_{1500} \lesssim -20$ are likely due to dust effects that have a similar magnitude at these luminosities and redshifts (see Fig. 1 of Wu & Kravtsov 2024). In addition, the figure also shows theoretical estimates from Sun et al. (2023); Leung et al. (2023), as well as Kravtsov & Belokurov (2024) which uses the same model as this work for consistency.

Figure 1 also shows that the UV luminosity function at luminosities fainter than those probed by observations is quite steep ($\approx -1 \sim -2$, depending on the redshift, see Table 1 of Wu & Kravtsov 2024, for more details) illustrating the potentially large contribution of faint galaxies to the UV and ionizing photon budgets. Agreement with UV LF estimates at a vast range of redshift $z \in [5, 16]$ at $M_{1500} < -14$, and the fact that the model reproduces properties of $z = 0$ dwarf galaxies well (Kravtsov & Manwadkar 2022), including the luminosity function of Milky Way satellites down to the ultra-faint magnitudes (Manwadkar & Kravtsov 2022), means we can plausibly expect that the model UV LF can faithfully describe the evolution of the UV luminosities and contribution of ionizing flux from galaxies of luminosities fainter than the observational limit.

2.3. *Models for the escape fraction of ionizing photons*

In addition to computing $\dot{N}_{\rm ion}$, to compute the reionization history of the Universe we need to make assumptions about the value of the escape fraction of ionizing photons from galaxies ($f_{\rm esc}$). Such assumptions can be motivated by observations (e.g., Chisholm et al. 2022; Saldana-Lopez et al. 2023; Topping et al. 2022; Cullen et al. 2023; Lin et al. 2024; Saxena et al. 2024) or theoretical models of ionizing radiation propagation in galaxy formation simulations (e.g., Wise et al. 2014; Sharma et al. 2016; Kimm et al. 2017; Anderson et al. 2017; Rosdahl et al. 2022). However, both observational estimates and theoretical modeling of the escape fraction have large associated uncertainties.

Therefore, we adopt several models for $f_{\rm esc}$ that should reasonably bracket the possible trends. These models range from the simplest constant $f_{\rm esc}$ assumption to the models motivated by the correlations of $f_{\rm esc}$ with UV luminosity or specific star formation rate from observations and simulations.

1. In the first model, we assume a *constant* $f_{\rm esc}$ at all redshifts and luminosities.

2. In the second model, we adopt a strong dependence of $f_{\rm esc}$ on galaxy luminosity for galaxies with $-21 < M_{1500} < -15$: $f^{\rm eff}_{\rm esc} = f_{\rm esc}(M_{1500} = -21) \times 10^{0.62(M_{1500}+21)}$, where $f_{\rm esc}(M_{1500} = -21) = 1.91 \times 10^{-4}$ normalized the function so that $f_{\rm esc}$ would increase to 1 towards the faintest galaxies. At $M_{1500} > -15$ is kept constant at $f_{\rm esc} = 1$. This model approximates the evolution of $f_{\rm esc}$ and in simulations Anderson et al. (2017) and evolution of $\xi_{\rm ion}$ deduced for observed galaxies by Simmonds et al. (2024). This toy model illustrates how different the results would be in the case of a strong increase of $f_{\rm esc}$ with fainter luminosities. Note, however, that the luminosity dependence in this model is likely too strong and overestimates the contribution of dwarf galaxies to the ionizing budget, as it assumes that both $f_{\rm esc}$ and $\xi_{\rm ion}$ increase with decreasing luminosity, while observations indicate that $f_{\rm esc}$ and $\xi_{\rm ion}$ anti-correlate in high-z galaxies (Saxena et al. 2024), such that their product does not depend strongly on luminosity.

3. Our third model for $f_{\rm esc}$ is based on its correlation with specific star formation rate (sSFR) of galaxies found in the SPHINX20 simulations of galaxy formation. Specifically, (Rosdahl et al. 2022, see their Fig. 12) found that in these galaxies $f_{\rm esc}$ increases with increasing *maximum* $\rm sSFR_{10}$ estimated over 50 Myr before the current epoch:

$$\rm sSFR_{max,10} = \max_{50\,Myr} sSFR_{10}, \qquad (2)$$

where

$$\rm sSFR_{10} = \frac{SFR_{10}}{M_\star} = \frac{M_\star(age < 10\,Myr)/10\,Myr}{M_\star}, \qquad (3)$$

and $M_\star$ is the current stellar mass of the galaxy, and $\rm SFR_{10}$ is the star formation rate averaged over the past 10 Myr. Observationally, this timescale roughly corresponds to SFRs determined by Hα. Importantly, Rosdahl et al. (2022) showed that dependence of $f_{\rm esc}$ on $\rm sSFR_{max,10}$ is similar at different redshifts (see their Fig. 15, also reproduced in Figure 2 below). Thus, to model such dependence, we only need a single parametrization of the $f_{\rm esc}(\rm sSFR_{10})$.

Physically, this correlation likely reflects a link between escape fraction and starburst-induced feedback, as pointed out and discussed in many previous works (Heckman et al. 2011; Sharma et al. 2017; Faucher-Giguère 2020), although the processes shaping $f_{\rm esc}$ remain a matter of ongoing debate. Our third model thus is an example of a simulation-motivated scenario implementing such correlation of $f_{\rm esc}$ with $\rm sSFR_{max,10}$.

Analyzing the distributions of $f_{\rm esc}$ in the SPHINX simulations as a function of $\rm sSFR_{max,10}$, we found that it can be well approximated by a random variable $x = \log_{10} f_{\rm esc}$ drawn from a two-component (bi-modal) mixture distribution function, where the first model is described by the skew-normal distribution

$$p_1(x|\xi,\omega) = \frac{2}{\omega\sqrt{2\pi}} e^{-\frac{(x-\xi)^2}{2\omega^2}} \int_{-\infty}^{\alpha\frac{x-\xi}{\omega}} \frac{1}{\sqrt{2\pi}} e^{-\frac{t^2}{2}} dt \quad (4)$$

and the second model by the normal distribution

$$p_2(x|\mu,\sigma) = \frac{1}{\sigma\sqrt{2\pi}} e^{-\frac{(x-\mu)^2}{2\sigma^2}}. \quad (5)$$

In the approximation we fix $\alpha = -3$ and $\omega = 1.6$ and adopt the following dependencies for ξ, μ, σ on $\log_{10}\mathrm{sSFR}_{\mathrm{max},10}$:

$$\begin{aligned} \xi &= 1.7(\log_{10}\mathrm{sSFR}_{\mathrm{max},10} - 2) - 0.7 \\ \mu &= \log_{10}\mathrm{sSFR}_{\mathrm{max},10} - 2.3 \\ \sigma &= 0.45 - 0.35(\log_{10}\mathrm{sSFR}_{\mathrm{max},10} - 2). \end{aligned} \quad (6)$$

We assume that the distribution of galaxies is produced by the equal fractions (50%) of galaxies drawn from the two components). All drawn f_{esc} values are capped at $f_{\mathrm{esc}} = 1$.

Figure 2 compares the f_{esc} distributions of the SPHINX galaxies and values produced using this approximation. The solid lines with different colors show the medians of f_{esc} distributions of `SPHINX` galaxies at different redshifts, while the shaded regions show the 68th and 84th percentiles of the distribution of f_{esc} (at $z = 6$, the distributions at other z are similar). The thick dashed line shows the median, and the thinner dotted lines show the 68th and 84th percentiles of the distribution for the f_{esc} values produced using this approximation for the same $\mathrm{sSFR}_{\mathrm{max},10}$ values. The figure shows that the approximation matches the SPHINX simulation results at $\log_{10}\mathrm{sSFR}_{\mathrm{max},10} > 0$ reasonably well. Although the match is not as good at lower values of $\mathrm{sSFR}_{\mathrm{max},10}$, such galaxies contribute little to the ionizing photon budget due to their low f_{esc} values.

In the third f_{esc} model we use this approximation to assign f_{esc} values to model galaxies in our calculation using the $\mathrm{sSFR}_{\mathrm{max},10}$ values computed from the star formation history of each model galaxy, accounting for SFR stochasticity. Our calculations showed that when applying this model to calculate hydrogen ionization history, we found reionization occurring too late ($z \lesssim 5$), consistent with the somewhat late reionization in the actual SPHINX20 simulation (Rosdahl et al. 2022). However, a similar model in which f_{esc} of each galaxy retains the same dependencies on $\mathrm{sSFR}_{\mathrm{max},10}$ but is boosted by a factor of two provides a good match to existing observational constraints on reionization. We thus use this "boosted" version as our fiducial third f_{esc} model. Note that a boost of f_{esc} by such a factor implies a significant change in the distribution of neutral hydrogen in the simulations. At the same time, one could think about this change as a factor of two change of the uncertain intrinsic ionizing flux of stellar populations due, for example, to a different model of binary star population. f_{esc} values are capped at 1.

We propagate the ionizing photons from the aforementioned three f_{esc} models with the method outlined in Section 2.2, and present ionizing histories in Section 2.4.

2.4. *Modeling hydrogen ionization history*

To quantitatively model the hydrogen ionization history, we construct an ionizing flux $\dot{n}_{\mathrm{ion}}(M_{1500})$ as a function of M_{1500}, similarly to how we estimate model UV LF in Wu & Kravtsov (2024). We then use a polynomial fit to model the redshift evolution of the best-fit Schechter functional form parameters over $5 \le z \le 16$, also described in the previous work. The method is outlined here again in Appendix C, with the resulting parameters presented in Appendix D.

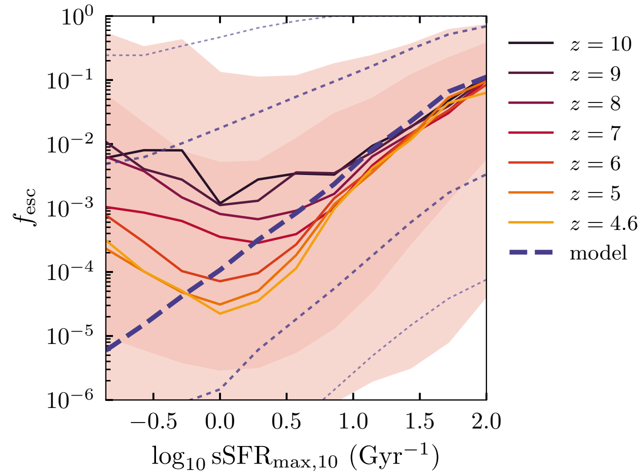

FIG. 2.— The f_{esc} distribution for galaxies in the `SPHINX` simulation, binned by maximum of the logarithm of the 10 Myr-averaged specific star formation rate sSFR_{10} measured over the past 50 Myr. The solid curves represent median f_{esc} values for different $\log_{10}\mathrm{sSFR}_{\mathrm{max},10}$ at different redshifts, and shaded regions correspond to 68th and 84th percentiles for SPHINX galaxies at $z = 6$ (the distributions at other z are similar). The dashed thick line represents the median, and the thinner dotted lines represent the 68th and 84th percentiles of the distribution for the same galaxies, but with $\log_{10}(f_{\mathrm{esc}})$ modeled using the approximation described in § 2.3.

With this parameterization of the time evolution of $\dot{n}_{\mathrm{ion}}(M_{1500})$ we can compute $\dot{n}_{\mathrm{ion}}(< M_{1500}^{\mathrm{lim}}, z)$, where we integrate ionizing photons at each redshift down to the luminosity limit $M_{1500} < -5$ on the faint end. This sums $\dot{N}_{\mathrm{ion}}$ flux contribution from all dwarf galaxies in our model, including those not currently observable by JWST at $M_{1500} > -13$. We also integrate to three different luminosity limits in the discussion Section 4.1, to investigate ionizing photon contributions from galaxies of different luminosities.

We use this function to solve for the volume-averaged hydrogen ionized fraction $Q(t)$ (Madau et al. 1999), rewriting it in a redshift-dependent form $Q(z)$ using $dt = -dz[H(z)(1+z)]^{-1}$:

$$\begin{aligned} \frac{dQ}{dz} &= -\frac{1}{H(z)(1+z)}\frac{dQ}{dt} \\ &= -\frac{1}{H(z)(1+z)}\left(\frac{\langle\dot{n}_{\mathrm{ion}}\rangle}{\langle n_H\rangle} - \frac{Q}{\bar{t}_{\mathrm{rec}}}\right), \end{aligned} \quad (7)$$

where $\langle\dot{n}_{\mathrm{ion}}\rangle = \dot{n}_{\mathrm{ion}}(< M_{1500}, z)$ is the ionizing photon production rate per unit proper volume, and $\langle n_H\rangle = 1.89\times10^{-7}(1+z)^3\mathrm{cm}^{-3}$ is the cosmological mean proper hydrogen density. We compute the "effective" recombination timescale $\bar{t}_{\mathrm{rec}}$ for $\mathrm{H_{II}}$ regions in the IGM using equations and assumptions of Madau et al. (2024) as:

$$1/\bar{t}_{\mathrm{rec}} \equiv (1+\chi)\alpha_B(T_0)\langle n_H\rangle C_R, \quad (8)$$

where $\alpha_B = 2.577\times10^{-13}\mathrm{cm}^3\mathrm{s}^{-1}$ is the combination coefficient computed with the fixed temperature of ionized gas of $T_0 = 10^4$K, $\chi \equiv Y/4X$, which assumes that helium is singly ionized at the same time as hydrogen, and doubly ionized only at later times.

We consider three redshift-dependent models of the IGM clumping factor $C_R(z)$. Following Madau et al. (2024),

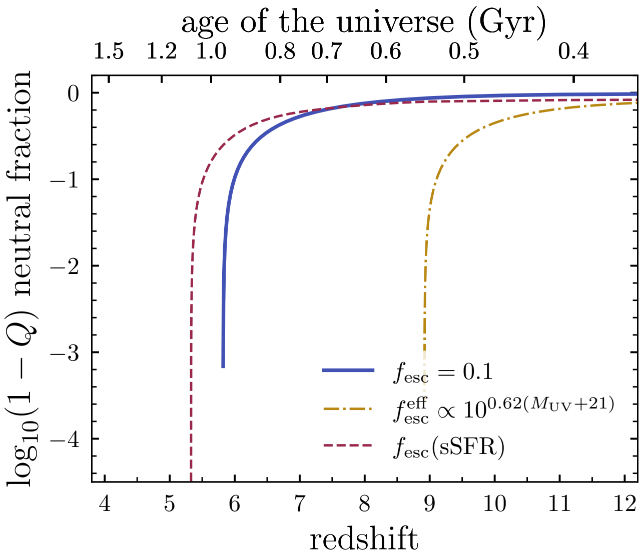

FIG. 3.— Reionization histories represented by the average neutral fraction $1 - Q$ of the intergalactic medium as a function of redshift and cosmic time. The curves show predictions from integrating Eq. 7 with three models for the ionizing photon escape fraction: a constant global $f_{\rm esc} = 0.1$ (blue); a model in which $f_{\rm esc} = f_{\rm esc}(M_{1500} = -21) \times 10^{0.62(M_{1500}+21)}$ increases monotonically for fainter galaxies (yellow), where $f_{\rm esc}(M_{1500} = -21) = 1.91 \times 10^{-4}$; and lastly the model where $f_{\rm esc}$ depends on specific star formation rate (red, see § 2.3). All models integrate galaxies at each redshift across the full luminosity range.

our fiducial model is a parameterization $C_R = 9.25 - 7.21 \log_{10}(1+z)$ calibrated from the radiation-hydrodynamic simulations of ionization inhomogeneities of Finlator et al. (2009) and Chen et al. (2020). We also consider two other models that bracket the upper and lower range of $C_R(z)$ in different simulations (e.g. Pawlik et al. 2009; Finlator et al. 2012; Shull et al. 2012; Kaurov & Gnedin 2015) shown in Fig. 2 of Davies et al. (2024). Specifically, the model that brackets the simulation results from above has C_R changing from 3 at $z > 10$ to 10 at $z \lesssim 6$: $C_R = \min\left[10, 3 + z^{-2.5}\exp(-0.3z + 7.4)\right]$, while the model that brackets simulation results from below is $C_R = 8 - 6.5 \log_{10}(1+z)$.

These three models of $C_R(z)$ are plotted in Figure 9 of the Appendix A. The effect of different clumping factor model choices on the hydrogen reionization history is discussed in Section 4.2, while all other calculations use the fiducial model.

3. RESULTS

3.1. *Model hydrogen ionization history compared to observations*

We integrate Equation 7 to a given z starting from a fully neutral universe ($Q = 0$) at $z_i = 16$. Figure 3 shows the resulting reionization histories represented by the average neutral fraction $1 - Q$ of the intergalactic medium with redshift and cosmic time, with the neutral fraction plotted on a logarithmic scale. This is done to emphasize the reionization epoch, $z_{\rm rei}$ at which the bulk of the intergalactic medium is ionized. The figure compares the three models for the escape fraction adopted in our study (see Section 2.3): a constant global $f_{\rm esc} = 0.1$, the strongly luminosity-dependent $f_{\rm esc}^{\rm eff}$ which increases linearly towards fainter galaxies, and the sSFR-dependent $f_{\rm esc}$ model motivated by the SPHINX galaxy formation simulation. All models include the ionizing flux contribution of all galaxies down $M_{1500} < -5$.

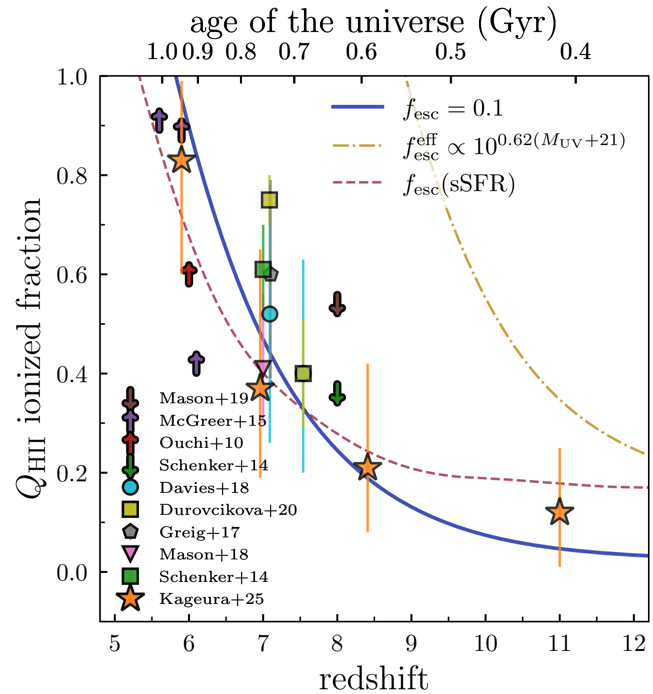

FIG. 4.— Hydrogen ionized fraction $Q_{\rm HII}(z)$ with redshift and cosmic time. The same curves representing $f_{\rm esc}$ models are shown as in Fig. 3 with the same colors. All models integrate galaxies at each redshift across the full luminosity range down to $M_{1500} < -5$. Observational measurements (points) and limits (arrows) are plotted from a compilation of Lyα, QSO, and IGM temperature measurements (e.g., Mason et al. 2019; McGreer et al. 2015; Ouchi et al. 2010; Schenker et al. 2014; Davies et al. 2018; Ďurovčíková et al. 2020; Greig et al. 2017; Mason et al. 2018; Kageura et al. 2025).

Figure 3 illustrates the high sensitivity of the reionization history to assumptions about the ionizing photon escape fraction. The model with luminosity-dependent escape fraction (yellow) reionizes around $z \sim 9$. This is too early to be compatible with observations (see below) and is consistent with conclusions of Muñoz et al. (2024) that the Universe would be reionized too early if escape fractions increases rapidly with decreasing galaxy luminosity. In the $f_{\rm esc} = 0.1$ model (blue) the universe reionizes at $z \sim 6$. The sSFR-dependent escape fraction model produces a reionization history quite similar to the $f_{\rm esc} = 0.1$ model. This shows that very different models of escape fraction may produce *similar* reionization histories.

Figure 4 compares reionization histories in these three models to observational constraints from observed Lyα, QSO, and IGM temperature measurements (e.g., Mason et al. 2019; McGreer et al. 2015; Ouchi et al. 2010; Schenker et al. 2014; Davies et al. 2018; Ďurovčíková et al. 2020; Greig et al. 2017; Mason et al. 2018; Kageura et al. 2025).

The figure shows that the model with $f_{\rm esc} = 0.1$ and the simulation-based sSFR-dependent $f_{\rm esc}$ model results are in good agreement with measurements of the IGM neutral fraction, while the model in which $f_{\rm esc}$ increases for fainter luminosities greatly overestimates the ionized fraction estimates at $z < 10$. Although not shown in the figure, we note that the shape of the $Q(z)$ line for the $f_{\rm esc} = 0.1$ model is also in good agreement with the parameterization: $Q = [(z_{\rm early} - z)/(z_{\rm early} - z_{\rm end})]^{\alpha}$ where $\alpha = 4$; $z_{\rm early} = 16$ is the redshift around which the first emitting sources form, and z_{end} is taken at the redshift where reionization draws to a close ($Q = 0.99$, $z = 5.77$), found to be a good fit to the CMB results in Planck Collaboration et al. (2016).

Interestingly, $Q(z)$ in the simulation-based sSFR-dependent f_{esc} model is similar to $f_{esc} = 0.1$. Despite this, the reionization history shows a sizeable fraction of ionized hydrogen – $Q_{HII} \approx 0.15 \sim 0.2$ – is produced at higher redsfhits ($z > 10$). Current observational constraints do not exclude such a scenario; and as we show below, such reionization history is consistent with the integrated optical depth constraints from the cosmic microwave background (CMB) measurements.

3.2. *Thomson optical depth*

Another key constraint on reionization histories is the Thomson electron optical depth due to the scattering of the CMB photons by free electrons produced during reionization, which can be computed as (Kuhlen & Faucher-Giguère 2012; Robertson et al. 2015; Robertson 2022):

$$\tau(z) = c\sigma_T \langle n_H \rangle \int_0^z dz' \frac{(1+z')^2}{H(z')} \left[1 + \frac{\eta Y}{4X}\right] Q_{HII}(z'), \quad (9)$$

where c is the speed of light, σ_T is the Thomson scattering cross section, $\langle n_H \rangle$ is the mean proper hydrogen density, and $Q_{HII}(z')$ is the volume-averaged ionized fraction computed in Section 3.1. The pre-factor accounts for free electrons contributed by helium at different ionization states. We adopt the assumption that helium is fully ionized ($\eta = 2$) at lower redshifts $z < 4$, and singly ionized ($\eta = 1$) at higher redshifts.

Figure 5 shows the $\tau(z)$ for the same three f_{esc} models considered above (see Section 2.3), which account for the contribution of model galaxies down to $M_{1500} < -5$. The predicted optical depths are compared to the $\tau = 0.054 \pm 0.014$ (2σ) constraints from the Planck Collaboration et al. (2020) measurements, as well as $\tau = 0.0626^{+0.0122}_{-0.0144} (2\sigma)$ from Heinrich & Hu (2021)'s more recent PC analysis of the same Planck data.

The figure shows that both the $f_{esc} = 0.1$ and sSFR-based f_{esc} models are consistent with the CMB constraints. The optical depth increase with redshift is similar in both model, but the integral τ is somewhat higher in the latter model due to the ionized hydrogen fraction tail at $z > 10$ in this model, seen in Figure 4. In contrast, the model with luminosity-dependent f_{esc} requires Thomson optical depth that is too large, thanks to the early reionization due to the large ionizing flux contribution of faint galaxies with high escape fractions. Together with the IGM neutral fraction constraints discussed in Section 3.1, it is clear that a monotonically increasing f_{esc} overestimates the dwarf contribution to the reionization.

4. DISCUSSION

4.1. *Contribution from galaxies of different luminosities*

Comparison of reionization histories and implied integral Thomson optical depth for CMB photon scattering in different models presented above highlights the high sensitivity of the model predictions to assumptions about the escape fraction dependence on galaxy properties.

The contribution of galaxies of different luminosities towards the ionizing photon budget is still somewhat uncertain (see, e.g., Finkelstein et al. 2019; Naidu et al. 2020; Wu & Kravtsov 2024). However, we show in this section that the effect of including galaxies of luminosity fainter than the observation limit is considerably smaller than the effect of different assumptions about f_{esc} – at least for the model employed

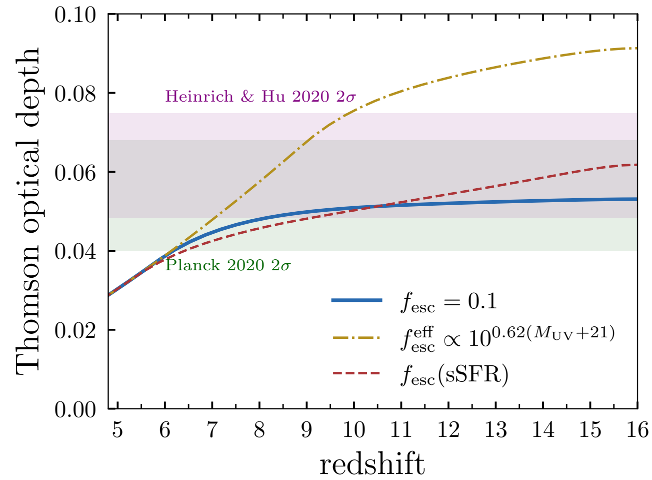

FIG. 5.— Thomson optical depth $\tau(z)$ as a function of redshift for the three ionizing escape fraction models: a constant $f_{esc} = 0.1$ integrated down to $M_{1500} < -5$ (blue), a model in which a model in which f_{esc} increases monotonically for fainter galaxies, and is normalized to 1 for the faintest galaxies (yellow), and the f_{esc} model depending on specific star formation rate (red). The colored bands shows the 2σ range of the opacity constraints measured by Planck Collaboration et al. (2020) and Heinrich & Hu (2021)'s reanalysis.

in our study, which reproduces properties of dwarf galaxies and their UV luminosities at $z \approx 7$, as indicated by their star formation histories (see Boylan-Kolchin et al. 2015; Weisz & Boylan-Kolchin 2017; Wu & Kravtsov 2024)

For example, Figure 6 shows reionization histories in the $f_{esc} = 0.1$ model accounting for only the ionizing photons produced by bright galaxies ($M_{1500} < -17$), by galaxies with $M_{1500} < -13$, and by all model galaxies $M_{1500} < -5$. We chose the constant $f_{esc} = 0.1$ model, given that it is in good agreement with all of the observational constraints in the case when we account for all galaxies ($M_{1500} < -5$, see Figure 4). The figure shows that including fainter galaxies accelerates the reionization process, in agreement with previous calculations (see, e.g., n_{ion} comparisons in Fig. 6 of Wu & Kravtsov (2024)). This is especially prominent at lower redshifts $z \lesssim 8$ where including dwarf galaxies with $M_{1500} > -13$ boosts the ionized fraction by almost 0.1, whereas the difference is not as significant at higher redshifts. Nevertheless, if the contribution of dwarf galaxies to the ionizing budget were neglected, to obtain the reionization history required to match observational constraints would only require increasing escape fraction from $f_{esc} = 0.1$ to $f_{esc} \approx 0.15$ (see, e.g., Robertson 2022).

The uncertainties in the overall contribution of faint galaxies to the ionizing photon production thus have a much smaller effect than the uncertainty in the relative escape fractions in galaxies of different luminosity (and other properties). This uncertainty is generic and is unlikely to be eliminated. Although attempts to characterize f_{esc} scaling with galaxy properties in high-resolution simulations continue (e.g., Wise et al. 2014; Kimm et al. 2017; Anderson et al. 2017; Rosdahl et al. 2022), the fidelity of each specific simulation is uncertain.

This reflects the daunting nature of the task: f_{esc} depends on the details of formation and spatial distribution of massive stars relative to the spatial distribution of neutral gas on an enormous range of scales (see, e.g., Howard et al. 2017, 2018; Menon et al. 2025) and can thus be easily affected both by the

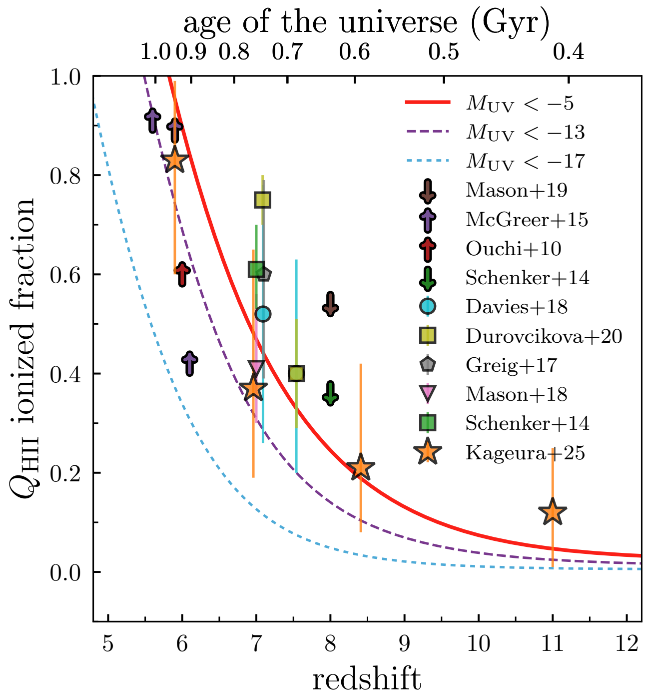

FIG. 6.— Hydrogen ionized fraction $Q_{\rm HII}(z)$ with redshift and cosmic time, assuming a fixed global escape fraction $f_{\rm esc} = 0.1$ and integrating over different faint-end limits of the galaxy UV magnitude: $M_{1500} < -17, -13$, and -5. Also shown are the same set of observational constraints as in Fig. 4, from a compilation of Lyα, QSO, and IGM temperature measurements.

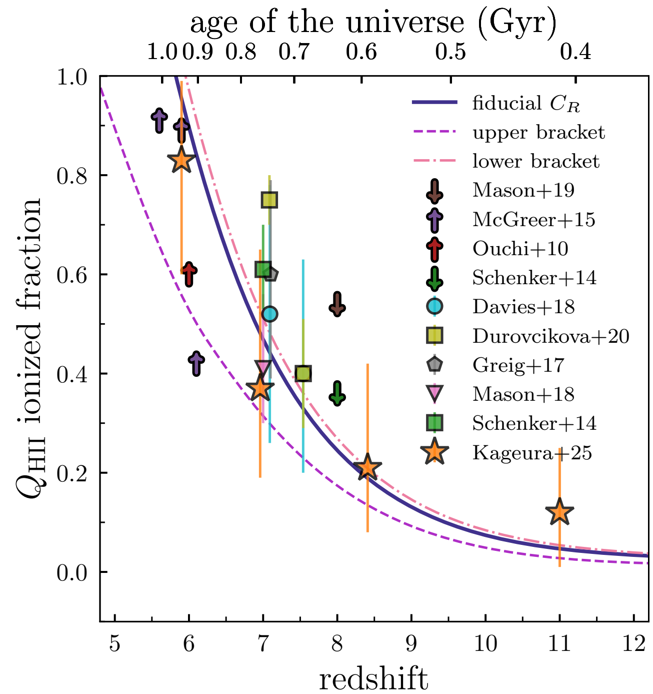

FIG. 7.— Hydrogen ionized fraction $Q_{\rm HII}(z)$ as a function of redshift and cosmic time, assuming a fixed global escape fraction $f_{\rm esc} = 0.1$ and accounting for the ionizing photons from all galaxies down to $M_{1500} < -5$. Reionization history is computed with a fiducial model for the IGM clumping factor model as a function of redshift $C_R(z)$ (blue) and two models bracketing results for $C_R(z)$ from a number of different simulations from above (purple) and below (pink line). The models are described in § 2.4 and 4.2. Also shown are the same set of observational constraints as in Fig. 4. The fiducial model and lower bracket models are close to each other and thus have similar reionization histories, while in the upper bracket model the Universe reionizes somewhat later.

insufficient fidelity in modeling star formation and feedback processes and by resolution effects.

At the same time, observational estimates of $f_{\rm esc}$ have their own uncertainties and a set of challenges. First, detailed measurements of escape fraction are difficult and are generally only available for lower redshift galaxies, not for the galaxies responsible for reionizing the Universe. Second, escape fractions for faint galaxies are inherently difficult or impossible to measure. Third, although some galaxy properties were found to correlate with $f_{\rm esc}$ and thus were proposed as proxies for its estimates (e.g., Chisholm et al. 2022), simulation-based tests indicate that such observational proxies may be biased or have a generally large scatter (e.g., Choustikov et al. 2024a,b).

Nevertheless, the utmost sensitivity of the reionization history modeling on the modeling of the ionizing photon escape fractions dictates that a combination of simulation-based inference and observations should be used to make progress. For example, despite the inherent challenges and uncertainties of the simulations discussed above, simulations can be used to test observational diagnostics or suggest the most promising properties of galaxies as proxies and related parametrizations of $f_{\rm esc}$. Promising efforts of this kind have recently been undertaken (e.g., Choustikov et al. 2025)

4.2. *Reionization history dependence on the IGM clumping factor*

The hydrogen reionization history is additionally sensitive to the assumed clumping factor, C_R, which affects the global hydrogen recombination rate. To illustrate the sensitivity of the reionization history to C_R, we show such histories for our fiducial model for $C_R(z)$ and the two models bracketing $C_R(z)$ in different simulations (see Section 2.4 for details).

Figure 7 shows the reionization histories for these three C_R models. As expected, a higher clumping factor delays reionization, since it requires a larger number of ionizing photons to fully reionize the Universe. Overall, however, the effect of different C_R prescriptions on the reionization history is modest and is much smaller than effect of choosing different models for $f_{\rm esc}$, or even the effects of including galaxies of different luminosities discussed above. This is true even though the range of values allowed between the models is likely larger than the actual range of plausible C_R values, as indicated by the study by Gnedin (2024), in which the clumping factor was modeled based on the combination of cosmological simulations and results of very high-resolution small-box simulations.

5. SUMMARY AND CONCLUSIONS

We presented model calculations of the reionization history of hydrogen using a galaxy formation model, which reproduces observational monochromatic (λ = 1500 Å) UV luminosity function measurements at $z \in [5, 16]$ and basic properties of both local dwarf galaxies (Manwadkar & Kravtsov 2022) and high-redshift galaxies (Kravtsov & Belokurov 2024; Wu & Kravtsov 2024). The star formation histories of model galaxies, including accounting for stochastic/bursty mode of star formation, have been used to estimate the Lyman continuum photon flux density function for galaxies at redshifts $z \in [5, 16]$ including the contribution of galaxies over the broad UV luminosity range from $M_{1500} \approx -25$ to $M_{1500} = -5$.[1]

We use the ionizing photon density functions along with different models for the escape fraction of ionizing photons, $f_{\rm esc}$, to study the effects of accounting galaxies of different UV luminosities and different assumptions about $f_{\rm esc}$ on the reionization history of the Universe, quantified by the hydrogen ionized fraction $Q_{\rm HII}(z)$ and its complementary neutral hydrogen fraction. Our main results and conclusions are as follows:

1. We show that including progressively fainter galaxies accelerates reionization (Figure 6). Accounting for the contribution of faint galaxies with UV luminosities $M_{1500} > -13$ in additional to bright galaxies results in the hydrogen reionization history, $Q_{\rm HII}(z)$, consistent with all current observational constraints for the *constant* ionizing photon escape fraction as low as $f_{\rm esc} = 0.1$ (Figures 4-5).

2. Comparing results of the constant $f_{\rm esc}$ model and two alternative models for $f_{\rm esc}$ dependence on galaxy properties, motivated by results of different galaxy formation simulations, shows high sensitivity of $Q_{\rm HII}(z)$ to the assumptions about the escape fraction behavior in the faint UV luminosity regime (Figures 3-4).

3. The model with strong luminosity dependence of $f_{\rm esc}$, which assigns high escape fractions to faint galaxies, results in early hydrogen reionization inconsistent with observational constraints on $Q_{\rm HII}(z)$ and the optical depth for the Thomson scattering of CMB photons, which is in agreement with conclusions of Muñoz et al. (2024).

4. The model in which $f_{\rm esc}$ follows a universal redshift-independent correlation with the recent maximum specific star formation rate, $\rm sSFR_{10,max}$, qualitatively similar to the correlation found in the SPHINX galaxy formation simulation, results in the reionization history in good agreement with existing observational constraints. Interestingly, this model produces a sizeable ionized hydrogen fraction of $Q_{\rm HII} \approx 0.15 - 0.2$ at redshifts $z = 8 - 12$ (Figure 4).

Our results show that although dwarf galaxies beyond the range of luminosities probed by HST and JWST produce a significant fraction of total hydrogen ionizing photons (as shown in our previous study Wu & Kravtsov 2024, see also Figure 6 above), their relative contribution depends sensitively on the assumptions about the escape fraction of ionizing photons for galaxies of different luminosity. The escape fraction of ionizing Lyman continuum photons and its dependence on galaxy properties at high redshifts is thus the main source of uncertainty in modeling details of hydrogen reionization, and should be the main focus of observational studies and galaxy formation simulations.

ACKNOWLEDGEMENTS

We are grateful to Brant Robertson, Nicholas Choustikov, Piero Madau, and the UChicago structure formation group for useful discussions. We also thank Nickolay Gnedin for discussions and useful detailed comments on the draft of this paper. ZW was supported by the University of Chicago CCRF's Quad Research Scholarship and University of California – San Diego's Astronomy & Astrophysics Achievement Award. The author is grateful to the University of Chicago for supporting his undergraduate thesis, which formed the basis for this work. The author thanks Hsiao-Wen Chen for valuable feedback as a member of his undergraduate thesis committee. AK was supported via the National Science Foundation grants AST-1911111 and AST-2408267, and NASA ATP grant 80NSSC20K0512.

Analyses presented in this paper were greatly aided by the following free software packages: `NumPy` (Harris et al. 2020), `SciPy` (Jones et al. 01), `Matplotlib` (Hunter 2007), `FSPS` (Conroy & Gunn 2010a) and its Python bindings package `Python-FSPS`[2], `BPASS` stellar population synthesis tables for ionizing luminosity Byrne et al. (2022), and `Colossus` cosmology package (Diemer 2018). We have also used the Astrophysics Data Service (`ADS`) and `arXiv` preprint repository extensively during this project and the writing of the paper.

DATA AVAILABILITY

A `GRUMPY` model implementation is available at `https://github.com/kibokov/GRUMPY`. Results of this paper can be reproduced from the fitting functions and parameters presented in Appendices C and D. The data used in the plots within this article are available on request to the corresponding author.

[1] The best fit parameters of the modified Schechter function describing the ionizing flux density of galaxies as a function of UV luminosity are provided in Table 3 in the Appendix D.

[2] `https://github.com/dfm/python-fsps`

REFERENCES

Anderson L., Governato F., Karcher M., Quinn T., Wadsley J., 2017, MNRAS, 468, 4077
Becker R. H., et al., 2001, AJ, 122, 2850
Bouwens R. J., et al., 2021, AJ, 162, 47
Bouwens R. J., Illingworth G., Ellis R. S., Oesch P., Stefanon M., 2022, ApJ, 940, 55
Bouwens R., Illingworth G., Oesch P., Stefanon M., Naidu R., van Leeuwen I., Magee D., 2023a, MNRAS, 523, 1009
Bouwens R. J., et al., 2023b, MNRAS, 523, 1036
Boylan-Kolchin M., Weisz D. R., Johnson B. D., Bullock J. S., Conroy C., Fitts A., 2015, MNRAS, 453, 1503
Byrne C. M., Stanway E. R., Eldridge J. J., McSwiney L., Townsend O. T., 2022, MNRAS, 512, 5329
Caplar N., Tacchella S., 2019, MNRAS, 487, 3845
Chen N., Doussot A., Trac H., Cen R., 2020, ApJ, 905, 132
Chisholm J., et al., 2022, MNRAS, 517, 5104
Choustikov N., et al., 2024a, MNRAS, 529, 3751
Choustikov N., et al., 2024b, MNRAS, 532, 2463
Choustikov N., Stiskalek R., Saxena A., Katz H., Devriendt J., Slyz A., Sub-department of Astrophysics U. o. O., 2025, MNRAS, 537, 2273
Conroy C., Gunn J. E., 2010a, FSPS: Flexible Stellar Population Synthesis, Astrophysics Source Code Library, record ascl:1010.043
Conroy C., Gunn J. E., 2010b, ApJ, 712, 833
Conroy C., Gunn J. E., White M., 2009, ApJ, 699, 486
Cullen F., et al., 2023, MNRAS, 520, 14
Davies F. B., et al., 2018, ApJ, 864, 142
Davies F. B., Bosman S. E. I., Furlanetto S. R., 2024, arXiv e-prints, p. arXiv:2406.18186
Diemer B., 2018, ApJS, 239, 35
Donnan C. T., et al., 2023, MNRAS, 518, 6011
Faucher-Giguère C.-A., 2020, MNRAS, 493, 1614
Finkelstein S. L., et al., 2019, ApJ, 879, 36
Finkelstein S. L., et al., 2022, ApJ, 940, L55
Finlator K., Özel F., Davé R., 2009, MNRAS, 393, 1090
Finlator K., Oh S. P., Özel F., Davé R., 2012, MNRAS, 427, 2464
Gnedin N. Y., 2000, ApJ, 535, 530
Gnedin N. Y., 2004, ApJ, 610, 9
Gnedin N. Y., 2016, ApJ, 825, L17
Gnedin N. Y., 2024, ApJ, 963, 150
Gnedin N. Y., Fan X., 2006, ApJ, 648, 1
Gnedin N. Y., Kaurov A. A., 2014, ApJ, 793, 30
Gnedin N. Y., Madau P., 2022, Living Reviews in Computational Astrophysics, 8, 3
Gnedin N. Y., Kravtsov A. V., Chen H.-W., 2008, ApJ, 672, 765
Greig B., Mesinger A., Haiman Z., Simcoe R. A., 2017, MNRAS, 466, 4239
Gunn J. E., Peterson B. A., 1965, ApJ, 142, 1633
Harikane Y., et al., 2023, ApJS, 265, 5
Harikane Y., Nakajima K., Ouchi M., Umeda H., Isobe Y., Ono Y., Xu Y., Zhang Y., 2024, ApJ, 960, 56
Harris C. R., et al., 2020, Nature, 585, 357–362
Heckman T. M., et al., 2011, ApJ, 730, 5
Heinrich C., Hu W., 2021, Phys. Rev. D, 104, 063505
Howard C., Pudritz R., Klessen R., 2017, ApJ, 834, 40
Howard C. S., Pudritz R. E., Harris W. E., Klessen R. S., 2018, MNRAS, 475, 3121
Hunter J. D., 2007, Computing In Science & Engineering, 9, 90
Jaacks J., Thompson R., Nagamine K., 2013, ApJ, 766, 94
Jones E., Oliphant T., Peterson P., et al., 2001–, SciPy: Open source scientific tools for Python, http://www.scipy.org/
Kageura Y., et al., 2025, arXiv e-prints, p. arXiv:2501.05834
Kannan R., Garaldi E., Smith A., Pakmor R., Springel V., Vogelsberger M., Hernquist L., 2022, MNRAS, 511, 4005
Kaurov A. A., Gnedin N. Y., 2015, ApJ, 810, 154
Kimm T., Katz H., Haehnelt M., Rosdahl J., Devriendt J., Slyz A., 2017, MNRAS, 466, 4826
Kravtsov A., Belokurov V., 2024, arXiv/2405.04578, submitted
Kravtsov A., Manwadkar V., 2022, MNRAS, 514, 2667
Kravtsov A., Wu Z., 2023, MNRAS, 525, 325
Kuhlen M., Faucher-Giguère C.-A., 2012, MNRAS, 423, 862
Leung G. C. K., et al., 2023, ApJ, 954, L46
Lewis J. S. W., Ocvirk P., Dubois Y., Aubert D., Chardin J., Gillet N., Thélie É., 2023, MNRAS, 519, 5987
Lin Y.-H., et al., 2024, MNRAS, 527, 4173
Ma X., Kasen D., Hopkins P. F., Faucher-Giguère C.-A., Quataert E., Kereš D., Murray N., 2015, MNRAS, 453, 960
Madau P., 2017, ApJ, 851, 50
Madau P., Haardt F., Rees M. J., 1999, ApJ, 514, 648
Madau P., Giallongo E., Grazian A., Haardt F., 2024, ApJ, 971, 75
Manwadkar V., Kravtsov A. V., 2022, MNRAS, 516, 3944
Mason C. A., Treu T., Dijkstra M., Mesinger A., Trenti M., Pentericci L., de Barros S., Vanzella E., 2018, ApJ, 856, 2
Mason C. A., Naidu R. P., Tacchella S., Leja J., 2019, MNRAS, 489, 2669
McGreer I. D., Mesinger A., D'Odorico V., 2015, MNRAS, 447, 499
McLeod D. J., et al., 2024, MNRAS, 527, 5004
Menon S. H., Burkhart B., Somerville R. S., Thompson T. A., Sternberg A., 2025, ApJ, 987, 12
Muñoz J. B., Mirocha J., Chisholm J., Furlanetto S. R., Mason C., 2024, arXiv e-prints, p. arXiv:2404.07250
Naidu R. P., Tacchella S., Mason C. A., Bose S., Oesch P. A., Conroy C., 2020, ApJ, 892, 109
O'Shea B. W., Wise J. H., Xu H., Norman M. L., 2015, ApJ, 807, L12
Ouchi M., et al., 2010, ApJ, 723, 869
Pallottini A., Ferrara A., 2023, A&A, 677, L4
Pan Y., Kravtsov A., 2023, arXiv e-prints, p. arXiv:2310.08636
Pawlik A. H., Schaye J., van Scherpenzeel E., 2009, MNRAS, 394, 1812
Pérez-González P. G., et al., 2023, ApJ, 951, L1
Planck Collaboration et al., 2016, A&A, 596, A108
Planck Collaboration et al., 2020, A&A, 641, A6
Robertson B. E., 2022, ARA&A, 60, 121
Robertson B. E., Ellis R. S., Furlanetto S. R., Dunlop J. S., 2015, ApJ, 802, L19
Robertson B., et al., 2024, ApJ, 970, 31
Rosdahl J., et al., 2022, MNRAS, 515, 2386
Saldana-Lopez A., et al., 2023, MNRAS, 522, 6295
Saxena A., et al., 2024, A&A, 684, A84
Schenker M. A., Ellis R. S., Konidaris N. P., Stark D. P., 2014, ApJ, 795, 20
Sharma M., Theuns T., Frenk C., Bower R., Crain R., Schaller M., Schaye J., 2016, MNRAS, 458, L94
Sharma M., Theuns T., Frenk C., Bower R. G., Crain R. A., Schaller M., Schaye J., 2017, MNRAS, 468, 2176
Shull J. M., Harness A., Trenti M., Smith B. D., 2012, ApJ, 747, 100
Simmonds C., et al., 2024, MNRAS, 527, 6139
Sokasian A., Abel T., Hernquist L., 2003, MNRAS, 340, 473
Sun G., Faucher-Giguère C.-A., Hayward C. C., Shen X., Wetzel A., Cochrane R. K., 2023, ApJ, 955, L35
Tacchella S., Forbes J. C., Caplar N., 2020, MNRAS, 497, 698
Topping M. W., Stark D. P., Endsley R., Plat A., Whitler L., Chen Z., Charlot S., 2022, ApJ, 941, 153
Weisz D. R., Boylan-Kolchin M., 2017, MNRAS, 469, L83
Wise J. H., Demchenko V. G., Halicek M. T., Norman M. L., Turk M. J., Abel T., Smith B. D., 2014, MNRAS, 442, 2560
Wu Z., Kravtsov A., 2024, The Open Journal of Astrophysics, 7, 56
Yue B., Ferrara A., Xu Y., 2016, MNRAS, 463, 1968
Ďurovčíková D., Katz H., Bosman S. E. I., Davies F. B., Devriendt J., Slyz A., 2020, MNRAS, 493, 4256

APPENDIX

A. $f_{\rm esc}$ AND C_R MODELS

In this section, we include visualizations of the escape fraction $f_{\rm esc}$ and the IGM clumping factor C_R models we use in this work.

Figure 8 shows the two of the three $f_{\rm esc}$ models we adopt with respect to galaxy luminosity M_{1500}: a constant global $f_{\rm esc} = 0.1$ (blue), and a model in which $f_{\rm esc} = f_{\rm esc}(M_{1500} = -21) \times 10^{0.62(M_{1500}+21)}$ increases monotonically for fainter galaxies (yellow), where $f_{\rm esc}(M_{1500} = -21) = 1.91 \times 10^{-4}$. The third model where $f_{\rm esc}$ depends on specific star formation rate cannot be plotted with M_{1500}, and is presented in Figure 2 instead. For details, see Section 2.3.

Figure 9 shows the three models $C_R(z)$ considered in this study. For details on our choices of models, see Section 2.4. The effect of different C_R assumptions is discussed in Section 4.2.

B. STOCHASTIC FORMATION PARAMETERS

Our star formation model used GRUMPY with specific modifications for modeling reionization as detailed in Wu & Kravtsov 2024, which has found a good match with $5 < z < 10$ galaxy

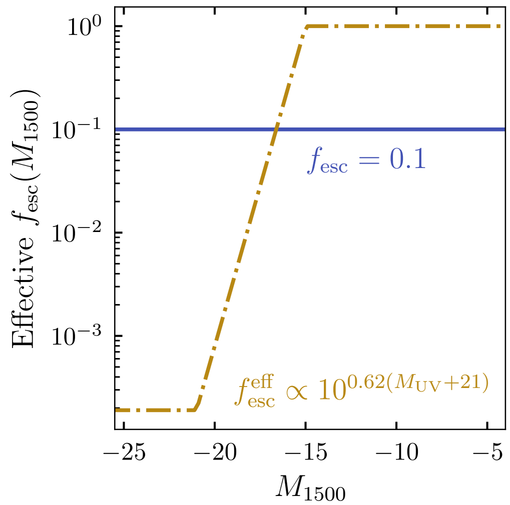

FIG. 8.— Two of the three $f_{\rm esc}$ models we adopt with respect to galaxy luminosity M_{1500}. For details, see § 2.3.

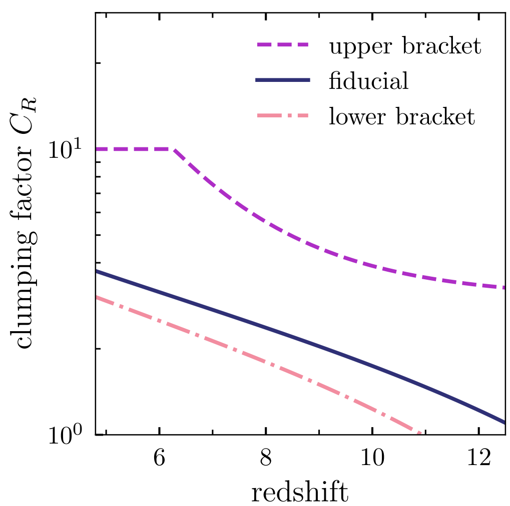

FIG. 9.— The IGM clumping factor C_R in three different $C_R(z)$ models considered in our study (see § 2.4 and 4.2 for details).

properties like the UV luminosity function. However, to account for the increasing effect of feedback in high redshift $z > 10$ galaxies, we modify our prescription of bursty star formation in line with Kravtsov & Belokurov (2024), which adopted a SFR stochasticity σ_Δ increasing with redshift. We follow Caplar & Tacchella (2019) and use the PSD of the form $\mathrm{PSD}(f) = \sigma_\Delta^2[1 + (\tau_{\rm break} f)^\alpha]^{-1}$, where σ_Δ characterizes the amplitude of the SFR variability over long time scales and $\tau_{\rm break}$ characterizes the timescale over which the random numbers are effectively uncorrelated. Parameter α controls the slope of the PSD at high frequencies (short time scales). In our models, we fix the slope α and $\tau_{\rm break}$ to the values $\alpha = 2$ and $\tau_{\rm break} = 100$ Myr, which are physically motivated by the time scales of gas evolution and star formation in giant molecular clouds in a typical ISM (see Tacchella et al. 2020, for a detailed discussion). For $z = 5-10$, we use $\sigma_\Delta = 0.1$ consistent with the typical amount of SFR stochasticity in host halos of observed galaxies at these redshifts. While for $z > 10$ we take σ_Δ values consistent with Kravtsov & Belokurov (2024). The specific parameters per redshift are summarized in Table 1.

TABLE 1
STOCHASTICITY PARAMETERS USED FOR GALAXY MODELS OF DIFFERENT REDSHIFTS $z = 5-16$, CONSISTENT WITH KRAVTSOV & BELOKUROV (2024).

z	5 – 10	11	12	13	14	16
$z_{\rm init}$	25	35	35	35	35	35
σ_Δ	0.1	0.15	0.15	0.16	0.18	0.25

TABLE 2
BEST-FIT PARAMETERS FOR JAACKS ET AL. (2013)'S MODIFIED SCHECHTER FUNCTION TO OUR STOCHASTIC UV LF AT $z = 5-16$. THE LAST COLUMN $\alpha - \beta$ SHOWS THE EFFECTIVE FAINT END LF SLOPE.

z	$\log_{10}\phi_*$ Mpc^{-3}	$M_{1500,*}$	$M_{1500,t}$	α	β	$\alpha-\beta$
5	-2.640	-23.268	-17.513	-0.453	0.744	-1.197
6	-3.544	-23.736	-18.668	-0.665	0.792	-1.458
7	-3.695	-23.502	-17.653	-0.702	0.789	-1.491
8	-4.246	-23.846	-17.957	-0.772	0.986	-1.758
9	-3.979	-22.604	-16.761	-0.786	0.793	-1.579
10	-4.428	-22.448	-16.812	-0.863	0.863	-1.726
11	-3.681	-22.546	-13.994	-0.756	0.577	-1.333
12	-3.611	-22.232	-12.348	-0.748	0.598	-1.346
13	-3.173	-22.387	-11.161	-0.661	0.655	-1.316
14	-2.393	-22.056	-10.012	-0.544	0.713	-1.257
16	-0.669	-22.229	-19.979	-0.229	0.926	-1.155

The corresponding scatter in the UV absolute magnitude is $\sigma_{\rm M_{UV}} \approx 0.75$ at low redshifts, increasing to ~ 2 at $z \approx 16$. These values are broadly consistent with the UV absolute magnitude fluctuations estimated in high-resolution zoom-in cosmological simulations at the same redshifts (Pallottini & Ferrara 2023; Sun et al. 2023, with slightly different values). We additionally note that adding stochasticity in our high-redshift galaxy model does not impact the late-time agreement with local universe observations. (see Kravtsov & Belokurov 2024, for further exploration of the effects of stochasticity in the context of the model we use)

C. UV LF MODIFIED SCHECHTER FITS

We approximate model UV luminosity functions with the modified Schechter functional form of Jaacks et al. (2013):

$$\Phi(L) = \phi_*\left(\frac{L}{L_*}\right)^\alpha \exp\left(-\frac{L}{L_*}\right)\left[1 + \left(\frac{L}{L_t}\right)^\beta\right]^{-1}, \quad \text{(C1)}$$

where ϕ_* and L_* are the normalization and characteristic luminosity of the bright end, respectively. Compared to the Schechter form, which has a fixed faint-end slope α, this form has a slope that can become progressively shallower or steeper around L_t and reaches the asymptotic slope of $\alpha-\beta$ at $L \ll L_t$.

We determine the best-fit parameters of the function by minimizing the least-squares differences between the functional form and model UV LF converted from the luminosity to absolute magnitude M_{1500} using the conversion

$$\begin{aligned} M_{1500} &= -2.5\log_{10}\frac{L_{1500}}{4\pi(10\,\mathrm{pc})^2} - 48.6 \\ &= -2.5\log_{10} L_{1500} + 51.59, \end{aligned} \quad \text{(C2)}$$

TABLE 3
BEST-FIT PARAMETERS FOR JAACKS ET AL. (2013)'S MODIFIED SCHECHTER FUNCTION TO THE IONIZING FLUX FUNCTION $\dot{n}_{\rm ion}$ AT $5 \leq z \leq 16$.

z	$\log_{10} 10^{-50}\dot{n}_{\rm ion,*}$	$M_{1500,*}$	$M_{1500,t}$	α	β
5	-3.914	-22.375	-15.184	-0.007	-0.738
6	-3.197	-22.067	-17.017	-0.170	-0.546
7	-2.670	-21.875	-16.883	-0.317	-0.639
8	-2.190	-21.810	-17.042	-0.510	-0.770
9	-0.652	-21.993	-16.783	-0.599	-0.822
10	-1.082	-21.571	-16.704	-0.707	-0.859
11	-0.786	-21.776	-16.462	-0.537	-0.697
12	-1.372	-22.852	-15.845	-0.606	-0.777
13	-0.818	-21.742	-10.486	-0.248	-0.646
14	-0.821	-21.892	-8.758	-0.215	-0.932
16	-0.036	-21.955	-8.966	-0.083	-1.124

where $L_{\rm UV}$ is the luminosity density at $\lambda = 1500\,\text{Å}$ in egs $\rm s^{-1}\,Hz^{-1}$.

The best-fit parameters for different redshifts $5 < z < 16$ are presented in Table 2. The table also shows the effect of reionization on the UV LF: it shows significant flattening of the faint-end slope $\alpha - \beta$ for redshifts $z \lesssim 6$ due to suppression of accretion caused by the UV heating of the intergalactic medium during and after reionization. In what follows, we present analytical fits to the emission rate of ionizing photons by UV magnitude, using the same modified Schechter form.

D. $n_{\rm ion}$ FUNCTIONAL FIT PARAMETER

We construct an ionizing flux function as a function of M_{1500}, $\dot{n}_{\rm ion}(M_{1500})$ similarly to how we estimate model UV LF (Section 2.2). Namely, we compute $\dot{n}_{\rm ion}(M_{1500})$ as a weighted histogram of halos in a box of a given comoving size $V_{\rm box}$ in bins of M_{1500} with weights given by $\dot{N}_{\rm ion}/(fV_{\rm box})$, where $\dot{N}_{\rm ion}$ is the Lyman continuum photom emission rate of each model galaxy and $f = f(M_{200c})$ is the fraction of selected halos in a given box.

This function can also be approximated analytically by the same modified Schechter function from Jaacks et al. (2013), in which ϕ_* in Equation C1 is replaced with $\dot{n}_{\rm ion,*}$. Fit parameters for the ionizing photon flux are shown in Table 3, analogous to M_{1500} UV LF parameters presented earlier in Table 2.

We provide an approximation for how best-fit parameters of the functional form evolve with redshift for $5 \leq z \leq 16$, so that one can reproduce our calculations of the LyC photon budget, and model the ionization history of the Universe by solving the time-evolution of $\dot{n}_{\rm ion}$ using Equation 7. Namely, we approximate the evolution of each parameter using third-order polynomials param $= a_0 + a_1 z + a_2 z^2 + a_3 z^3$. Figure 10 shows the polynomial fits for each parameter, while Table 4 presents the best-fit values of a_i coefficients.

This paper was built using the Open Journal of Astrophysics LaTeX template. The OJA is a journal which provides fast and easy peer review for new papers in the `astro-ph` section of the arXiv, making the reviewing process simpler for authors and referees alike. Learn more at http://astro.theoj.org.

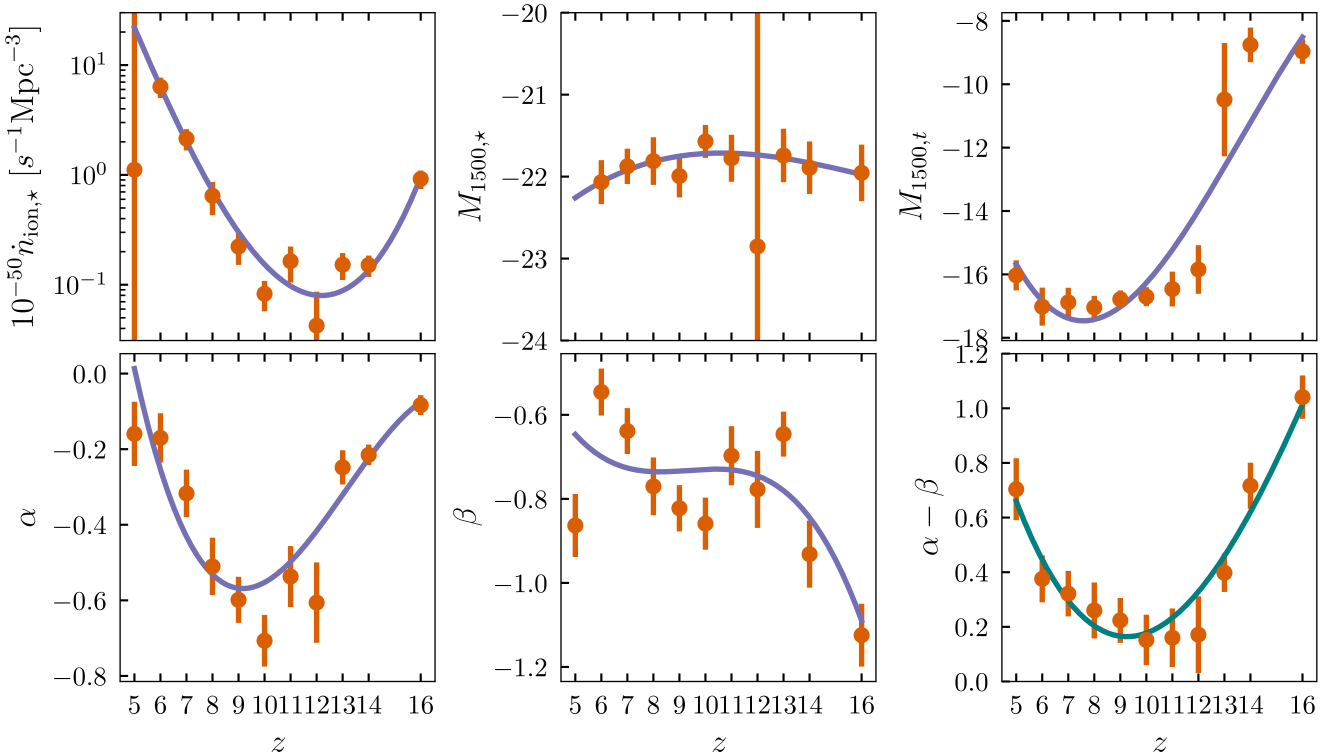

FIG. 10.— Coefficients of the third-order polynomial fit approximation to the evolution of the parameters of the Jaacks et al. (2013) analytical form to $\dot{n}_{\rm ion}(M_{1500})$ at $5 \leq z \leq 16$. The bottom right panel (green line) shows how the faint-end slope of the $\dot{n}_{\rm ion}$ functions change across redshifts $5 < z < 16$. The polynomial coefficients are presented in Table 4.

TABLE 4
COEFFICIENTS OF THE THIRD-ORDER POLYNOMIAL FIT APPROXIMATION TO THE EVOLUTION OF THE PARAMETERS OF THE JAACKS ET AL. (2013) APPROXIMATION TO $\dot{n}_{\rm ion}(M_{1500})$ WITH REDSHIFT AT $5 \leq z \leq 16$.

Parameters	a_3	a_2	a_1	a_0
$10^{-50}\dot{n}_{\rm ion,*}$	0.0024	-0.0242	-0.4948	4.1152
$M_{1500,*}$	0.0007	-0.0367	0.5284	-24.0759
$M_{1500,t}$	-0.0130	0.5310	-5.8082	1.7121
α	-0.0021	0.0824	-0.9830	3.1297
β	-0.0013	0.0365	-0.3356	0.2826